Dermatol Ther (Heidelb) (2025) 15:2865–2878
https://doi.org/10.1007/s13555-025-01504-0

ORIGINAL RESEARCH

High-Frequency Ultrasound Imaging for Stage III Cellulite: A Three-Subtype Structural Classification from an Observational Cohort Study

Dora Intagliata · Massimiliano Priolo · Paola Molinari

Received: June 12, 2025 / Accepted: July 17, 2025 / Published online: July 25, 2025

ABSTRACT

Introduction: Stage III cellulite is traditionally assessed through clinical inspection; however, visual scales often fail to capture the structural complexity of subcutaneous tissue. High-frequency ultrasound (HFUS) provides an objective, non-invasive method for visualizing the architecture of adipose tissue. This study aimed to develop and validate an ultrasound-based subclassification of stage III cellulite to improve diagnostic accuracy and facilitate personalized treatment strategies.

Methods: This observational cohort study included 150 female patients (ages 20–55 years, BMI 18–32 kg/m^2) with a clinical diagnosis of stage III cellulite. Two physicians independently performed clinical staging (3A/3B) using the Nürnberger–Müller scale. A single physician conducted HFUS examinations of the subgluteal and trochanteric regions using a 20-MHz probe. Ultrasound features, including fat thickness, echotexture, fibrosis, and edema, served to classify patients into three phenotypes: 3A, 3B, and mixed.

Results: HFUS identified 50 patients in each subtype. The mean superficial fat thickness was 4.8 ± 1.1 mm in 3A, 11.3 ± 2.4 mm in 3B, and 8.6 ± 3.4 mm in mixed subtype. Severe fibrosis occurred in 100.0% of patients with type 3B, was absent in type 3A, and was variable in the mixed type. Edema was mild in all patients with type 3A (100.0%), severe in 44.0% of those with type 3B, and variable in the mixed group. Discrepancies between clinical and ultrasound classifications appeared in 33.3% of cases. Agreement between classifications was moderate (Gwet's AC1 = 0.444; $p < 0.001$).

Conclusion: HFUS provides a valid and reproducible method for structurally assessing advanced cellulite. It enables the identification of a third, clinically unrecognized mixed phenotype, which has significant therapeutic implications by supporting more accurate treatment selection and improving treatment personalization.

Keywords: Cellulite; Ultrasonography; Subcutaneous fat; Diagnostic imaging; Edema; Fibrosis

Supplementary Information The online version contains supplementary material available at https://doi.org/10.1007/s13555-025-01504-0.

D. Intagliata (✉)
Poliambulatorio ID Future, Via Alcide De Gasperi, 66, Siracusa, Italy
e-mail: idmedicalsrl@gmail.com

M. Priolo
Aesthetic Medicine, Acqui Terme, Italy

P. Molinari
Studio Medicina Estetica, Modena, Italy

Key Summary Points

Why carry out this study?

Stage III cellulite affects the vast majority of post-pubertal women and has significant psychosocial and esthetic implications.

Conventional visual assessment methods do not capture the structural heterogeneity of subcutaneous tissue, which limits diagnostic precision and personalized treatment planning.

The purpose of this study was to investigate whether high-frequency ultrasound (HFUS) can identify reproducible structural subtypes within stage III cellulite to support a more individualized clinical approach.

What was learned from the study?

High-frequency ultrasound made it possible to classify stage III cellulite into three different morphological phenotypes: type 3A, type 3B, and a previously unrecognized mixed subtype.

The mixed phenotype, which combines features of both 3A and 3B, was identified in one-third of patients and is not detectable by clinical examination alone.

The agreement between the clinical and ultrasound-based classification was moderate, which emphasizes the additional diagnostic value of imaging.

INTRODUCTION

Cellulite, also known as edematous fibrosclerotic panniculopathy (EFP), is a multifactorial connective tissue disorder that affects approximately 85–98% of post-pubertal women [1]. Clinically, it presents as a dimpled or "orange peel" appearance of the skin, resulting from structural and microcirculatory alterations in the subcutaneous tissue [2–4]. Beyond its esthetic manifestations, cellulite imposes a significant psychosocial burden, adversely affecting body image and overall quality of life [5].

The pathophysiology of cellulite is complex, involving multiple interacting factors, such as hormonal influences, lymphatic and venous stasis, fibrotic septal contraction, adipocyte hypertrophy, and local inflammation [3, 4]. These mechanisms contribute to changes at the dermal and subcutaneous interface, ultimately causing deformation of the skin surface. Although commonly regarded as a cosmetic concern, growing evidence indicates that cellulite reflects deeper histological and vascular alterations, underscoring the need for accurate and objective diagnostic tools [5, 6].

Traditionally, the diagnosis of cellulite relies on visual and tactile inspection, supported by standardized classification systems, such as the Nürnberger–Müller classification and the Hexsel and Abreu scales [7, 8]. While these tools offer useful clinical benchmarks, they are inherently limited in their ability to assess deeper structural abnormalities within adipose and fibrotic compartments [9]. Current staging models often oversimplify the heterogeneity of stage III cellulite by treating it as a uniform entity. This approach fails to capture the substantial interindividual variability in tissue morphology, an important factor that can influence both treatment planning and therapeutic outcomes.

High-frequency ultrasound (HFUS) has recently emerged as a valuable, non-invasive imaging modality for visualizing the architecture of subcutaneous fat and connective tissue in vivo [6–8]. It enables detailed assessment of both superficial and deep fat layers and facilitates the identification of key echostructural abnormalities, such as fibrotic septa and interstitial edema, which are often undetectable through physical examination [5, 9]. Incorporating HFUS into cellulite assessment holds promise for enhancing clinical understanding and management of the condition. By providing reproducible, real-time visualization of the dermis and hypodermis, HFUS offers objective and quantifiable parameters for monitoring cellulite progression and evaluating treatment outcomes. Its capacity to detect morphological patterns associated with edema, fibrosis, and

fat remodeling adds anatomical and functional depth to otherwise superficial clinical assessments [5–7].

HFUS provides a detailed assessment of the superficial soft tissues by distinguishing three anatomically and functionally distinct layers: the dermo-epidermal complex (DEC), composed of the epidermis and dermis; the subcutaneous tissue (SUBC), which includes fat lobules and fibrous structures and can be further subdivided into superficial and deep compartments; and the deep fascia, a hyperechoic linear structure that separates the subcutaneous tissue from the underlying muscle. Within the SUBC, HFUS allows visualization of specific histological components, such as hypoechoic fat lobules, hyperechoic fibrous septa that provide mechanical support, and the superficial fascia, which delineates the boundary between the superficial and deep layers of the subcutaneous tissue [6].

The present study aims to introduce a novel ultrasound-based subclassification of stage III cellulite, grounded in detailed sonographic assessment of superficial subcutaneous adipose tissue in anatomical regions commonly affected by cellulite. By correlating these imaging features with specific therapeutic needs, this classification is expected to support the personalized selection of injectables, needle lengths, and medical devices, thereby improving both the safety and efficacy of cellulite treatment strategies.

METHODS

This monocentric, observational cohort study aimed to develop an ultrasound-based subclassification system for stage III cellulite. Patients were consecutively recruited from two outpatient esthetic clinics between November 2024 and January 2025. Clinical classification according to the Nürnberger–Müller classification was performed independently by both physicians involved in the study, with each blinded to the other's assessment. In contrast, all ultrasound examinations were conducted by a single trained physician using the same high-frequency device, ensuring uniform image acquisition and interpretation across all patients. No formal ethical application was submitted, as current Italian regulations do not require ethics committee approval for non-interventional studies conducted in private esthetic settings and not involving drugs, medical devices, or invasive procedures. The study was conducted in accordance with the principles of the Declaration of Helsinki. All participants gave their written informed consent, including permission for photographic documentation. Personal data was anonymized and processed in compliance with the General Data Protection Regulation (GDPR, EU 2016/679). Additionally, this study adheres to the STROBE guidelines for observational research.

Participants

Female patients aged 20 to 55 years with a clinical diagnosis of stage III cellulite, based on the Nürnberger–Müller classification, were consecutively recruited. Inclusion criteria were patients with (1) BMI between 18 and 32 kg/m^2, (2) regular menstrual cycles, and (3) no esthetic treatments in the preceding 6 months. Patients who (1) were pregnant, (2) were breastfeeding, (3) had hormonal disorders, (4) had dermatological conditions affecting the lower limbs, or (5) were using medications known to influence water retention or fat metabolism were excluded. A total of 150 participants were enrolled in the study after providing written consent, including permission for photographic documentation.

To minimize hormonal fluctuations, all ultrasound examinations were scheduled between the 7th and 12th day of the menstrual cycle, corresponding to the late follicular phase. This time frame was selected on the basis of evidence indicating that estrogen exerts less influence on subcutaneous tissue morphology during this period. Each patient underwent a standardized clinical assessment performed independently by two trained esthetic physicians. Clinical photographs of the affected areas (posterior thigh and buttock region) were taken under standardized lighting and positioning conditions. HFUS examinations were performed with a wireless 20-MHz linear probe (Clarius L20 HD3,

Clarius Mobile Health, Vancouver, Canada) with a maximum scanning depth of 4 cm. This device is optimized for high-resolution imaging of superficial structures and was used to visualize the dermis, superficial adipose tissue, and fibrous components within the subcutaneous compartment. All scans were performed with a gain setting of 50% and a depth range of 2–4 cm. This frequency range provides excellent axial resolution (< 50 µm), which is essential for the accurate detection of microstructural features of cellulite such as fibrotic septa, echotextural inhomogeneity, and interlobular edema. To ensure consistency, all examinations were conducted by a single trained operator—a physician with more than 15 years of experience in body contouring techniques and more than 4 years of specific training in HFUS. The ultrasound probe was positioned perpendicular to the skin over marked depressions in the subgluteal and trochanteric regions (Fig. 1). All ultrasound examinations were performed according to standard imaging practices, taking care to minimize transducer pressure on the skin.

Two specific depths were assessed:

- At 2 cm depth, the superficial adipose tissue above the superficial fascia, including the presence of fibrotic septa and edema, was evaluated.
- At 4 cm depth, the deep adipose tissue below the superficial fascia, focusing on fibrotic structures and compartmentalization, was evaluated.

Ultrasound features were analyzed in terms of:

- Thickness of the superficial and deep adipose tissue layers
- Echogenicity and echotextural homogeneity
- Distribution and density of fibrous septa
- Presence of vascular structures (assessed via color Doppler)

Edema was operationally defined as the presence of hypoechoic zones in the subcutaneous tissue indicating interstitial fluid accumulation. These areas lacked organized structure and appeared as regions of low echogenicity that were clearly distinguishable from hyperechoic linear fibrous septa as a result of their deformability under light probing pressure. All scans were performed in both the longitudinal and transverse planes to allow three-dimensional characterization of edema distribution. Although we did not classify specific fluid patterns such as the "cobblestone" or "snowfall" signs commonly used in the assessment of lymphedema with low-frequency probes [6], the identification of interlobular hypoechoic fluid was used to assist in phenotypic classification into edematous, fibrotic, or mixed subtypes. The criteria for ultrasound assessment and classification were based on the methodological framework proposed by Mlosek and Malinowska [7], which demonstrated the diagnostic relevance of combining HFUS-derived structural measurements with clinical staging to improve the objectivity and reproducibility of cellulite assessment.

To anatomically differentiate the examined subcutaneous layers, HFUS imaging focused on two primary compartments: the superficial adipose tissue (located above the superficial fascia)

Fig. 1 Ultrasound probe positioning for the evaluation of the gluteal region. A Longitudinal orientation of the transducer with the marker pointing cranially (↑). B Transverse orientation of the transducer with the marker pointing to the patient's right (←). *SUP* superficial subcutaneous tissue, *SUBC* subcutaneous tissue, *DEC* dermo-epidermal complex

and the deep adipose tissue (located below the superficial fascia). Figure 2a illustrates the echographic structure and boundaries of the superficial fat layer, which is particularly important for defining cellulite phenotypes. In contrast, deep adipose tissue, as shown in Fig. 2b, exhibited relatively consistent morphology across all participants and was not considered diagnostic within the current classification framework.

Classification Algorithm

On the basis of ultrasound characteristics, patients were categorized into three subtypes:

- Stage 3A: superficial adipose thickness less than 7 mm, few fibrotic bands, relatively homogeneous tissue structure, and presence of hypoechoic edema zones.
- Stage 3B: superficial adipose thickness greater than 7 mm, dense fibrotic network, marked echostructural inhomogeneity and thick collagen fibers.
- Mixed stage 3: clinical features of stage III combined with ultrasound findings partially overlapping with other stages, requiring integrative interpretation.

To standardize data collection and improve methodological rigor, the authors developed a special ultrasound assessment form that was used throughout the study. The complete form can be found in Supplementary Materials S1.

Variables and Definitions

The primary outcome was the identification of ultrasound-based subtypes within stage III cellulite. Secondary outcomes included the associations between ultrasound classifications and ultrasound patterns.

Bias and Standardization Measures

To minimize selection and measurement bias, the study enrolled patients consecutively and standardized ultrasound settings across all sessions. All assessments were blinded to clinical grading. The device was calibrated daily.

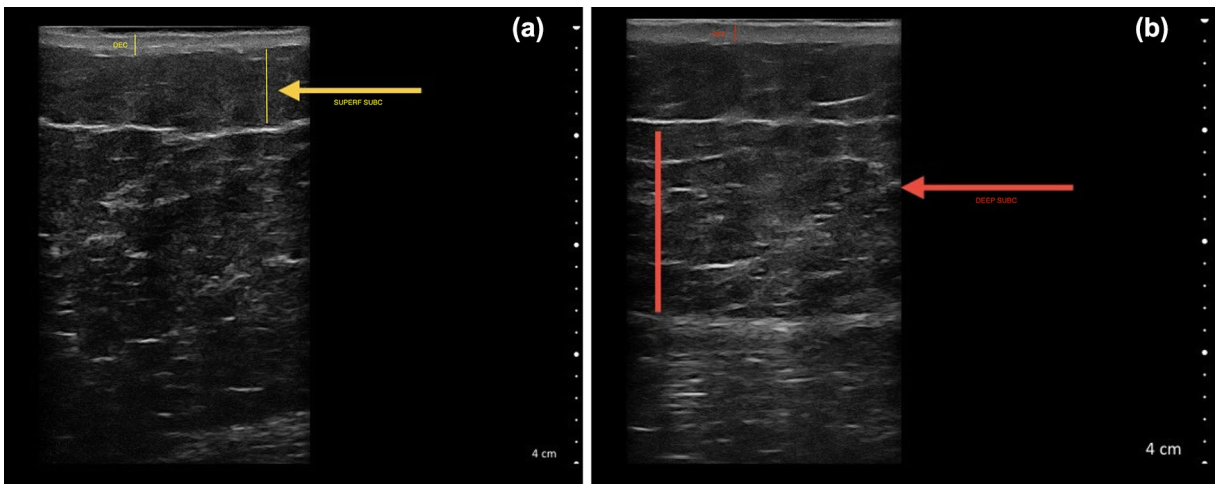

Fig. 2 Representative ultrasound images of cellulite phenotypes. **a** Ultrasound image showing the superficial adipose tissue (indicated by the yellow arrow) located between the dermo-hypodermal junction and the superficial fascia. This layer is central to the proposed classification due to its morphological variability across different cellulite phenotypes. **b** Ultrasound image depicting the deep adipose tissue (indicated by the red arrow), extending from the superficial fascia to the muscle fascia. This layer exhibited uniform morphology in all subjects examined and was not considered diagnostic in the current classification approach. *SUP.* *SUBC* superficial subcutaneous tissue, *DEC* dermo-epidermal complex

Statistical Analysis

Descriptive statistics were presented as mean ± standard deviation (SD) along with median and interquartile range (IQR: 25th to 75th percentile) for continuous variables and as relative frequencies and percentages for categorical variables. The distribution of continuous data was assessed using the Shapiro–Wilk test. As a result of the non-normal distribution, comparisons between clinical subgroups were performed using the Mann–Whitney *U* test, while Fisher's exact test was applied for categorical variables.

To assess agreement between the clinical (Nürnberger–Müller classification) [8] and ultrasound-based classifications, several inter-rater agreement coefficients were calculated, including Cohen's kappa, Gwet's AC1, Brennan and Prediger's coefficient, and Krippendorff's alpha. The strength of agreement was interpreted using standard thresholds, with values above 0.20 considered at least moderate and values above 0.40 considered substantial.

The use of multiple agreement coefficients aimed to address methodological differences and potential limitations inherent in individual indices. Specifically, although Cohen's kappa is widely used, it is sensitive to trait prevalence and imbalances in marginal distributions. Therefore, Gwet's AC1 and Brennan and Prediger's coefficient were included to provide more robust estimates under such conditions. All coefficients were calculated on the basis of classification into the 3A, 3B, or mixed subgroups. Statistical significance was tested under the null hypothesis of random agreement, with all indices yielding statistically significant results at the 5% level ($p < 0.05$), supporting the internal consistency and diagnostic value of ultrasound-based stratification.

Differences among the three ultrasound-defined subgroups (3A, 3B, and mixed) were analyzed using the Kruskal–Wallis test for continuous variables, followed by post hoc pairwise comparisons using Dunn's procedure. For categorical variables, Fisher's exact test was applied. Statistical significance was defined as a two-sided p value < 0.05. All analyses were performed using STATA19 (StataCorp, College Station, TX, USA).

RESULTS

A total of 150 female patients aged 20 to 55 years (mean age 37.1 ± 9.1 years) with clinically confirmed stage III cellulite were included in the study. The average body weight was 63.7 ± 5.9 kg, and the average BMI was 23.0 ± 3.2, with most patients falling in the normal weight category. Specifically, 66.7% of patients were classified as normal weight (BMI 18.5–24.9), 29.3% as pre-obese (BMI 25.0–29.9), and 3.3% as underweight (BMI < 18.5); only 0.7% were categorized as obese (BMI ≥ 30.0). All participants were classified according to the Nürnberger–Müller scale and equally divided into two clinical subgroups: 75 patients as type 3A and 75 as type 3B, based on visual inspection and palpation conducted by two independent assessors.

Group 3B patients were older (39.9 ± 8.2 vs. 34.4 ± 9.2 years; $p < 0.001$), heavier (65.4 ± 5.8 vs. 62.1 ± 5.5 kg; $p < 0.001$), and had a higher BMI (23.8 ± 2.9 vs. 22.3 ± 3.3; $p = 0.002$) compared to group 3A. Clinically, group 3B showed a significantly higher prevalence of pain on palpation (76.0% vs. 36.0%; $p < 0.001$), nodule formation (86.7% vs. 9.3%; $p < 0.001$), venous stasis (42.7% vs. 17.3%; $p < 0.001$), and fluid retention (72.0% vs. 56.0%; $p = 0.031$). No significant differences were observed regarding hormonal changes ($p = 0.497$), while the use of pharmacological treatments showed a modest but statistically significant variation ($p = 0.029$). Complete patient characteristics are reported in Table 1.

Ultrasound vs. Clinical Classification: Concordance Analysis

To quantify agreement between the clinical and ultrasound-based classifications, several interrater agreement metrics were calculated (Table 2). The overall percentage agreement between the two methods was 79.2%, indicating a substantial proportion of concordant classifications. Among the reliability coefficients, Gwet's AC1 demonstrated the highest value

Table 1 Patient characteristics

Variables	Total sample ($n = 150$)	3A ($n = 75$)	3B ($n = 75$)	p value
Age	37.1 (9.1) [36; 29–45]	34.4 (9.2) [33; 27–40]	39.9 (8.2) [38; 33–46]	< 0.001
Weight (kg)	63.7 (5.9) [63; 59–68]	62.1 (5.5) [61; 59–65]	65.4 (5.8) [64; 61–69]	< 0.001
Body mass index (BMI)	23 (3.2) [23; 20–25.5]	22.3 (3.3) [22; 19.5–25]	23.8 (2.9) [24; 22–26]	0.002
Underweight (< 18.5)	5 (3.3)	5 (6.7)	0 (0)	0.051
Normal weight (18.5–24.9)	100 (66.7)	51 (68)	49 (65.3)	
Pre-obesity (25.0–29.9)	44 (29.3)	19 (25.3)	25 (33.3)	
Obesity (≥ 30.0)	1 (0.7)	0 (0.0)	1 (1.3)	
Presence of pain on palpation	84 (56.0)	27 (36.0)	57 (76.0)	< 0.001
Presence of nodules	72 (48.0)	7 (9.3)	65 (86.7)	< 0.001
Venous stasis	45 (30.0)	13 (17.3)	32 (42.7)	< 0.001
Retention	96 (64.0)	42 (56.0)	54 (72.0)	0.031
Hormonal alterations				
No	147 (98.0)	73 (97.3)	74 (98.7)	0.497
Endometriosis	1 (0.7)	0 (0.0)	1 (1.3)	
Polycystic ovary	2 (1.3)	2 (2.7)	0 (0.0)	
Drug therapies				
None	142 (94.7)	73 (97.3)	69 (92.0)	0.029
Antihypertensive	2 (1.3)	0 (0.0)	2 (2.7)	
Cardioaspirin	1 (0.7)	0 (0.0)	1 (1.3)	
Levothyroxine	3 (2.0)	0 (0.0)	3 (4.0)	
Contraceptive therapy	2 (1.3)	2 (2.7)	0 (0.0)	

Table 2 Agreement

Coefficient	Estimate	Standard error	t	p value	95% confidence interval
Percent agreement	0.792	0.030	26.4	< 0.001	0.733–0.851
Brennan and Prediger	0.375	0.090	4.2	< 0.001	0.197–0.553
Cohen/Conger's kappa	0.286	0.062	4.6	< 0.001	0.164–0.408
Gwet's AC1	0.444	0.092	4.8	< 0.001	0.263–0.626
Krippendorff's alpha	0.203	0.085	2.4	0.018	0.035–0.371

(0.444), indicating moderate agreement with relatively high stability. This was followed by Brennan and Prediger's coefficient (0.375) and Cohen/Conger's kappa (0.286). Krippendorff's alpha yielded the lowest coefficient (0.203) but remained statistically significant ($p = 0.018$), underscoring the robustness of the classification method. All coefficients reached statistical significance ($p < 0.05$), supporting the internal consistency and reliability of the ultrasound classification protocol. Notably, the clinical classification included only two categories (3A and 3B), whereas the ultrasound-based classification introduced a third distinct category (mixed). For concordance analysis, the dichotomous clinical model was compared with this trichotomous ultrasound system. Despite this categorical asymmetry, all interrater coefficients produced statistically significant results ($p < 0.05$), confirming the robustness and diagnostic value of the ultrasound-based stratification.

Concordance between the initial clinical classification (Nürnberger–Müller) and the ultrasound-based classification was observed in 66.7% of cases for both 3A and 3B patients (Table 3). However, in approximately one-third of the cohort, ultrasound findings revealed a hybrid structural phenotype that did not correspond to the initial clinical assignment. These patients were reclassified into the mixed subtype, characterized by overlapping features of both 3A and 3B.

Table 3 Concordance analysis

	Ultrasound classification			
	3A	**3B**	**Mixed**	**Total**
Nürnberger–Müller scale				
3A	50 (66.7)	0 (0.00)	25 (33.3)	75 (100.0)
3B	0 (0.00)	50 (66.7)	25 (33.3)	75 (100.0)
Total	50 (33.3)	50 (33.3)	50 (33.3)	150 (100.0)

Ultrasound-Based Differentiation of Subtypes

Ultrasound examination revealed several statistically significant differences among the three subgroups defined by ultrasound classification (3A, 3B, and mixed) (Table 4). Specifically, the thickness of the superficial adipose tissue was significantly lower in group 3A (mean 4.8 ± 1.1 mm), higher in group 3B (11.3 ± 2.4 mm), and moderate in the mixed subgroup (8.6 ± 3.4 mm) ($p < 0.001$). Regarding edema, 100.0% of patients in groups 3A and 3B exhibited distinct and mutually exclusive patterns. Patients in group 3A presented only mild edema, whereas those in group 3B displayed either moderate (56.0%) or severe (44.0%) edema. Notably, 60.0% of patients in the mixed subgroup showed edema, indicating overlapping structural features. These differences were statistically significant ($p < 0.001$). The degree of fibrosis also differed significantly across groups. All patients in group 3A exhibited mild fibrosis, while all patients in group 3B demonstrated severe fibrosis. The mixed subgroup, however, displayed a heterogeneous distribution of fibrosis grades, further supporting its transitional characterization ($p < 0.001$). Finally, there were almost no fibrotic sprouts in group 3A (96.0%), whereas group 3B showed a high prevalence of moderate (42.0%) and large (58.0%) fibrotic formations ($p < 0.001$).

Representative ultrasound images for each identified phenotype are presented in Figs. 3, 4, and 5. Subtype 3A (Fig. 3a, b) exhibited a homogeneous superficial fat layer with reduced thickness (< 7 mm) and minimal fibrotic bands. In contrast, subtype 3B (Fig. 4a, b) showed marked echostructural inhomogeneity, characterized by thick fibrotic septa and increased adipose thickness (> 7 mm). The mixed subtype (Fig. 5a, b) demonstrated hybrid features, including irregular echogenicity and variable patterns of fibrosis and edema, underscoring its transitional nature.

DISCUSSION

This prospective observational study proposed and validated a novel ultrasound-based subclassification of stage III cellulite, identifying

Table 4 Ultrasound parameters comparison

	Total sample ($n = 150$)	3A ($n = 50$)	3B ($n = 50$)	Mixed ($n = 50$)	p value
Surface adipose Tissue thickness (mm)	8.2 (3.7) [7.5; 5–11.4]	4.8 (1.1) [4.85; 3.9–5.4]	11.3 (2.4) [11.35; 9.7–13.5]	8.6 (3.4) [8.85; 5.2–11.6]	< 0.001
Edema					
Absent	20 (13.3)	0 (0.0)	0 (0.0)	20 (40.0)	< 0.001
Light	66 (44)	50 (100.0)	0 (0.0)	16 (32.0)	
Moderate	28 (18.7)	0 (0.0)	28 (56.0)	0 (0.0)	
Severe	36 (24.0)	0 (0.0)	22 (44.0)	14 (28.0)	
Fibrosis					
Absent	14 (9.3)	0 (0.0)	0 (0.0)	14 (28.0)	< 0.001
Light	59 (39.3)	50 (100.0)	0 (0.0)	9 (18.0)	
Moderate	18 (12)	0 (0.0)	0 (0.0)	18 (36.0)	
Severe	59 (39.3)	0 (0.0)	50 (100.0)	9 (18.0)	
Fibrotic sprouts					
Absent	62 (41.3)	48 (96)	0 (0.0)	14 (28.0)	< 0.001
Minor	2 (1.3)	2 (4.0)	0 (0.0)	0 (0.0)	
Moderate	43 (28.7)	0 (0.0)	21 (42.0)	22 (44.0)	
Large	43 (28.7)	0 (0.0)	29 (58.0)	14 (28.0)	

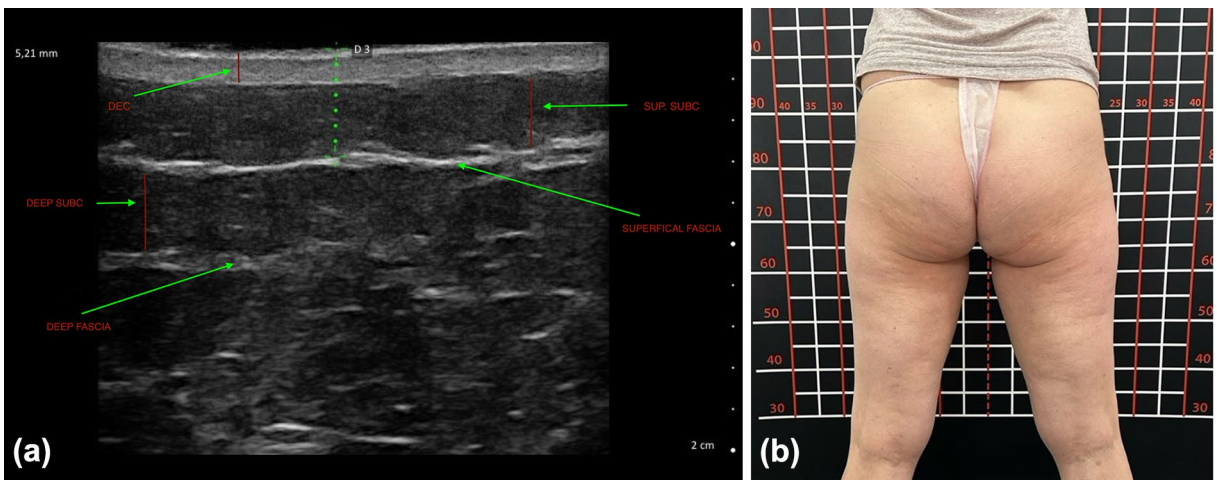

Fig. 3 Patient with a stage 3A phenotype. **a** Ultrasound image showing a superficial fat layer of low thickness (< 7 mm) with homogeneous echotexture and minimal fibrotic septa. **b** The clinical image showing mild dimpling without nodules, indicative of predominant edema and mild fibrosis. *SUP. SUBC* superficial subcutaneous tissue, *SUBC* subcutaneous tissue, *DEC* dermo-epidermal complex

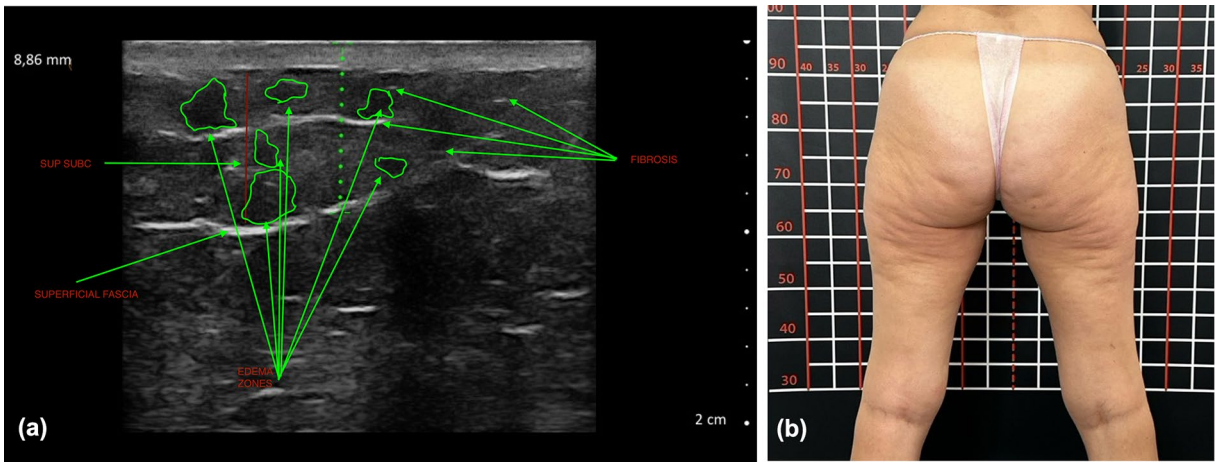

Fig. 4 Patient with a stage 3B phenotype. **a** Ultrasound image showing a thickened superficial fat layer (>7 mm), with marked echostructural inhomogeneity and dense hyperechoic fibrotic septa. **b** The clinical image showing increased pitting, nodularity, and irregularities on the skin surface, characteristic of advanced fibrosis. *SUP. SUBC* superficial subcutaneous tissue, *SUBC* subcutaneous tissue, *DEC* dermo-epidermal complex

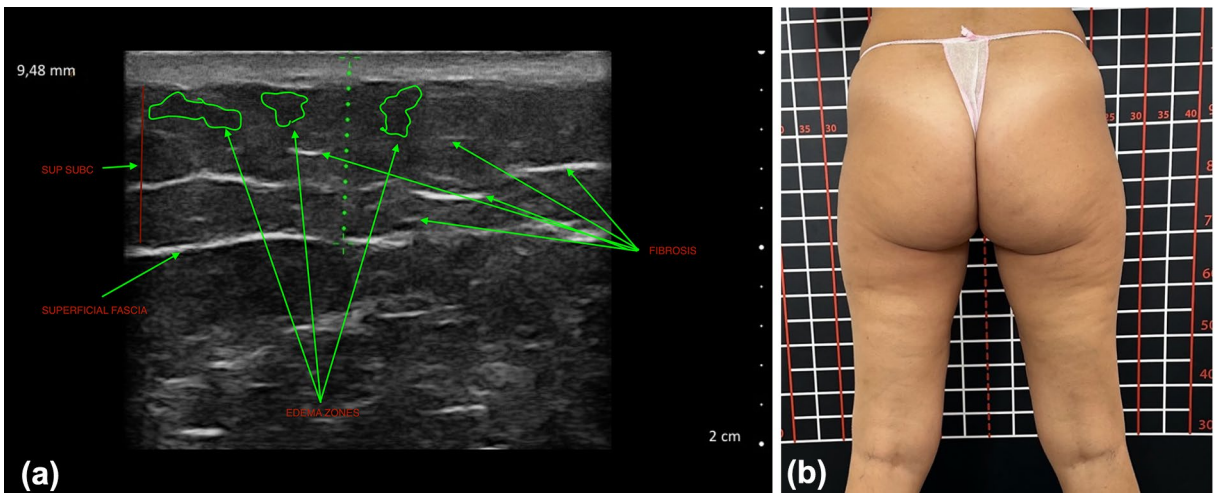

Fig. 5 Patient with a mixed phenotype. **a** Ultrasound image showing heterogeneous fat thickness and irregular echogenicity, with both mild and marked fibrotic septa. **b** The clinical photograph displaying asymmetry and overlapping features of stages 3A and 3B, highlighting the transitional nature of this phenotype. *SUP. SUBC* superficial subcutaneous tissue, *SUBC* subcutaneous tissue, *DEC* dermo-epidermal complex

three phenotypes, 3A, 3B, and mixed, based on quantifiable structural features of subcutaneous tissue. The findings suggest that conventional clinical classification systems, such as the Nürnberger–Müller scale, inadequately capture the morphological heterogeneity of advanced EFP. The recognition of a distinct mixed phenotype highlights the superior diagnostic resolution of HFUS, which enables the detection of transitional morphotypes not discernible through standard visual inspection.

The significant demographic and clinical differences observed between the groups clinically classified as 3A and 3B reflect the expected

variability within stage III cellulite. These differences support the hypothesis that the clinical subgroups represent genuinely distinct phenotypes whose differentiation can be further validated and refined through HFUS analysis.

Compared to clinical assessment alone, HFUS demonstrated significantly greater discriminatory power in evaluating fibrotic septa, interstitial edema, and adipose tissue thickness. These parameters varied markedly between subgroups, revealing a continuous spectrum of structural changes within stage III cellulite. For example, subtype 3B was characterized by pronounced fibrotic reorganization and increased adiposity relative to 3A, whereas the mixed phenotype exhibited overlapping features, supporting the conceptualization of stage III as a spectrum rather than a uniform entity [9–11].

Although sonographic imaging has previously been utilized in cellulite assessment, this study is the first to propose a rigorously defined and reproducible framework for subclassification within a single clinical stage. Multiple concordance indices confirmed the internal consistency and reliability of the proposed model. Importantly, nearly one-third of patients initially classified as 3A or 3B were reclassified as mixed on the basis of HFUS findings, underscoring the potential for misclassification when relying solely on visual assessment [7, 10].

The present results confirm and extend previous studies by Mlosek and Malinowska, who highlighted the diagnostic value of HFUS in quantifying dermal and hypodermal alterations and detecting echogenic fibrotic bands [7]. Similarly, Whipple et al. demonstrated that fibrous septa, particularly those arising obliquely from the superficial fascia, play a central role in the pathogenesis of cellulite depression [11]. Our study builds upon these findings by showing that these features not only indicate disease severity but also possess significant discriminatory power for phenotypic stratification.

Moreover, the existing literature supports the utility of HFUS in monitoring treatment outcomes [10]. Our results suggest that a morphologically based classification system can enhance therapeutic precision. For instance, subtype 3A, characterized by minimal fibrosis and predominant edema, may respond more favorably to superficial drainage and lipolytic therapies. Conversely, phenotype 3B may require more invasive interventions targeting fibrous septa, such as subcision or enzymatic lysis [12, 13].

The observed morphological differences further highlight the heterogeneity within stage III cellulite. These findings validate the diagnostic criteria applied, enhance the transparency of the classification system, and offer clinicians practical reference standards. The inclusion of representative HFUS images not only aids dissemination but also facilitates reproducibility across diverse clinical settings.

Study Limitations, Strengths, and Future Perspectives

This study has several limitations. Among the major limitations, the monocentric, nonrandomized design and recruitment from two single private esthetic centers may restrict the generalizability of the findings. Furthermore, the absence of histopathological correlation limits the direct validation of ultrasound findings, despite similar correlations reported in the literature [9]. Minor limitations include the lack of longitudinal follow-up, which prevents evaluation of the prognostic or therapeutic implications of the identified phenotypes, and the relatively small sample size ($n = 150$), which, although adequate for internal comparisons, may limit external applicability across different clinical settings and populations.

Another methodological consideration concerns the potential influence of transducer pressure on subcutaneous fat measurements. Although the suspension technique, which consists of minimizing the compression caused by the transducer by suspending the probe with a generous amount of gel, was not used in the current protocol, its importance in preserving tissue morphology in the assessment of lymphedema and subcutaneous water content has been well established [14]. In our study, all ultrasound examinations were performed in accordance with standard high-frequency imaging procedures, ensuring minimal contact pressure to avoid the development of artifacts. Nevertheless, future studies could benefit

from the formal introduction of the suspension technique to further standardize image acquisition and improve reproducibility, especially in the quantitative assessment of superficial fat layers.

Future research should focus on externally validating this classification model across multicenter and ethnically diverse populations. Correlating ultrasound-based subtypes with histologic features, patient-reported outcomes, and therapeutic responses will be essential to establishing clinical utility. Furthermore, integrating HFUS with artificial intelligence-based pattern recognition may enhance diagnostic accuracy and reduce operator dependency. Longitudinal studies are also warranted to evaluate the prognostic value of these subtypes in predicting treatment outcomes and disease progression.

Despite limitations, the study is strengthened by its methodological rigor, including standardized patient selection, scheduling examinations during the late follicular phase to minimize hormonal variability, and employing multiple indices of interrater agreement. The proposed classification system is feasible using commercially available HFUS devices, enhancing its potential for widespread clinical implementation. Moreover, the identified morphological patterns align with the existing histologic and MRI-based literature [7, 9], supporting both the biological plausibility and the broader clinical relevance of the classification.

A particularly noteworthy strength of this study is the identification and characterization of the mixed subtype. This ultrasound phenotype, defined by the coexistence of features typical of both subtypes 3A and 3B, often eludes detection through clinical assessment alone. Sole reliance on visual inspection may lead to misclassification, resulting in suboptimal or inappropriate treatment decisions. For example, superficial techniques might be inappropriately applied to fibrotic areas or invasive methods might be used in edematous tissue with minimal fibrosis, both scenarios that could contribute to treatment resistance or failure. This risk underscores the diagnostic power of HFUS and reinforces the added value of the proposed classification system in advancing precision medicine within esthetic practice.

The results of this study provide a preliminary sonostructural framework for the classification of stage III cellulite into different morphological subtypes. This classification can help to develop personalized therapeutic strategies by highlighting the predominant pathological component. Recognizing these ultrasound patterns in clinical practice could facilitate a more accurate assessment of patients and the selection of targeted interventions. Although our results are preliminary, they suggest that HFUS could play a role not only in diagnosis but also in tailoring and monitoring the efficacy of cellulite treatments.

CONCLUSION

This study introduces a novel, clinically applicable ultrasound-based subclassification of stage III cellulite. By delineating and validating three distinct phenotypic morphotypes, it provides improved diagnostic precision and supports a personalized, anatomically oriented therapeutic approach. Incorporating HFUS into routine esthetic practice can overcome the inherent limitations of visually based classification and lay the foundation for future research on individualized cellulite treatment.

ACKNOWLEDGEMENTS

We thank the participants of the study.

Author Contributions. Dora Intagliata conceived and designed the study, performed all ultrasound examinations, carried out the data analysis and was primarily responsible for the drafting of the original manuscript. Massimiliano Priolo contributed substantially to the study design, performed data collection, and provided critical revisions to the intellectual content. Paola Molinari contributed to the statistical analysis, helped with the literature review and interpretation of the results, and supported the revision of the manuscript. All authors have reviewed and approved the final version of the manuscript and agree to be responsible for all aspects of the work.

Funding. No Funding or sponsorship was received for this study or publication of this article. The Rapid Service Fee was funded by the authors.

Data Availability. The dataset analyzed during the current study is not publicly available due to restrictions imposed by Italian privacy law, which prohibits the dissemination of personally identifiable information. Data may be available from the corresponding author upon reasonable request and subject to compliance with the General Data Protection Regulation (EU 2016/679).

Declarations

Conflict of Interest. Dora Intagliata, Massimiliano Priolo, and Paola Molinari declare that they have no conflicts of interest to disclose.

Ethical Approval. This was a non-interventional, non-pharmacological observational study conducted in a private clinical setting, without the use of drugs, medical devices, or invasive or diagnostic procedures beyond routine care. Under Italian law, only pharmacological observational studies or studies with medical devices are subject to ethics committee approval and mandatory registration with the AIFA (Italian Medicines Agency) via the Registro Studi Osservazionali (RSO). This is clearly specified in the Ministerial Decree of November 30, 2021 (Italian Ministry of Health) and in AIFA Determination No. 425/2024 – Guidelines on Observational Studies (published on March 7, 2024). All participants have given written informed consent before inclusion in the study, in accordance with the principles of the Declaration of Helsinki.

REFERENCES

1. Nobile V, Cestone E, Puoci F, et al. In vitro and in vivo study on humans of natural compound synergy as a multifunctional approach to cellulite-derived skin imperfections. Cosmetics. 2020;7:48.
2. Bass LS, Hibler BP, Khalifian S, et al. Cellulite pathophysiology and psychosocial implications. Clin Cosmet Investig Dermatol. 2023;49:S2–7.
3. Bennardo L, Fusco I, Cuciti C, et al. Microwave therapy for cellulite: an effective non-invasive treatment. J Clin Med. 2022;11:515.
4. Hartman N, Almukhtar R, Wood ES, Fabi SG. Collagenase *Clostridium histolyticum*-Aaes injections for volumetric change of cellulite dimples and gluteal contouring. Dermatol Surg. 2023;49:383–6.
5. Bauer J, Hoq MN, Mulcahy J, et al. Implementation of artificial intelligence and non-contact infrared thermography for prediction and personalized automatic identification of different stages of cellulite. EPMA J. 2020;11:17–29.
6. Ricci V, Ricci C, Cocco G, et al. From histology to sonography in skin and superficial tissue disorders: EURO-MUSCULUS/USPRM* approach. Pathol Res Pract. 2022;237:154003.
7. Mlosek K, Malinowska S. High-frequency ultrasound in the assessment of cellulite—correlation between ultrasound-derived measurements, clinical assessment, and Nürnberger–Müller scale scores. Diagnostics. 2024;14:1878.
8. Nürnberger F, Müller G. So-called cellulite: an invented disease. J Dermatol Surg. 1978;4:221–9.
9. Scarano A, Petrini M, Sbarbati A, et al. Pilot study of histology aspect of cellulite in seventy patients who differ in BMI and cellulite grading. J Cosmet Dermatol. 2021;20:4024–31.

10. Sylwia M, Krzysztof MR. Efficacy of intradermal mesotherapy in cellulite reduction—conventional and high-frequency ultrasound monitoring results. J Cosmet Laser Ther. 2017;19:320–4.

11. Whipple LA, Fournier C, Heiman AJ, et al. The anatomical basis of cellulite dimple formation: an ultrasound-based examination. Plast Reconstr Surg. 2021;148:375e-e381.

12. Sadick NS, Goldman MP, Liu G, et al. Collagenase *Clostridium histolyticum* for the treatment of edematous fibrosclerotic panniculopathy (cellulite): a randomized trial. Dermatol Surg. 2019;45:1047–56.

13. Sant'Ana EMC, Pianez LRG, Custódio FS, Guidi RM, Freitas JNd. Effectiveness of carboxytherapy in the treatment of cellulite in healthy women: a pilot study. Clin Cosmet Investig Dermatol. 2016;9:183–90.

14. Ricci V, Ricci C, Gervasoni F, et al. From physical to ultrasound examination in lymphedema: a novel dynamic approach. J Ultrasound. 2022;25:757–63.